Scanning Microscopy

Volume 1995
Number 9 *Luminescence*

Article 4

1995

Cathodoluminescence of Rare Earth Doped Zircons. II. Relationship Between the Distribution of the Doping Elements and the Contrasts of Images

G. Rémond
BRGM, Orléans, France, guy@valcofim.fr

P. Blanc
Université P. et M. Curie, Paris

F. Cesbron
ESEM, Orléans, France

D. Ohnenstetter
Vandoeuvre-lés-Nancy, France

O. Rouer
CRSCM CNRS, Orléans, France

Scanning Microscopy Supplement 9, 1995 (Pages 57-76) 0892-953X/95$5.00+.25
Scanning Microscopy International, Chicago (AMF O'Hare), IL 60666 USA

CATHODOLUMINESCENCE OF RARE EARTH DOPED ZIRCONS. II. RELATIONSHIP BETWEEN THE DISTRIBUTION OF THE DOPING ELEMENTS AND THE CONTRASTS OF IMAGES

G. Rémond[1,*], P. Blanc[2], F. Cesbron[3], D. Ohnenstetter[4], O. Rouer[5]

[1]B.R.G.M., Orléans, France; [2]URA-CNRS 1761, Université P. et M. Curie, Paris, France; [3]URA-CNRS 1366, E.S.E.M., Orléans, France; [4]C.R.P.G., C.N.R.S., Vandoeuvre-lès-Nancy, France; and [5]C.R.S.C.M., C.N.R.S., Orléans, France

Abstract

Cathodoluminescence (CL) color photographs using an optical CL microscope with a cold cathode electron gun are compared with non-spectrally resolved (polychromatic) and selected wavelength CL images obtained by means of a scanning electron microscope equipped with a CL spectrometer. It is the aim of this paper to show how the interpretation of the contrasts of CL images depends on the knowledge of the CL photon energy distributions participating to the observed contrasts as well as the matrix effects modifying the number of emitted photons compared to that of generated photons. It is shown that the impurities different from the rare earth elements (REE) activators are responsible for charge trapping mechanisms leading to the development of internal electric fields modifying the energy and spatial distribution of the electrons within the insulators and consequently modifying the relative intensities of the intrinsic (host lattice) emission and characteristic emission of a REE activator. In addition, the mechanisms of production of photons must be better understood before trying to express the CL intensity of a monochromatic line as a function of the corresponding REE activator.

Key Words: REE-doped synthetic zircon, cathodoluminescence microscopy, doping element distribution, charge trapping centers, intrinsic and extrinsic emission induced contrasts.

*Address for correspondence and present address:
G. Rémond
32 Avenue de la Mouillere,
45100 Orléans, France
Telephone number: 33-38-66 66 62
E-mail: guy@valcofim.fr

Introduction

Cathodoluminescence (CL) microscopy has been intensively used to reveal heterogeneities within natural or synthetic crystals which are apparently homogeneous when observed by optical microscopy or scanning electron microscopy (SEM) as reviewed, among others, by Rémond *et al.* (1992) for wide bandgap crystals, and by Bresse *et al.* (1996) for semiconductors. As CL properties of crystals are usually related to the presence of small amounts of impurities, many comparisons between CL, X-ray, and backscattered and secondary electron images have been reported (see the review, Rémond *et al.*, 1992). Hanchar and Rundnick (1995) combined CL and backscattered electron imaging for revealing hidden structures in zircon ($ZrSiO_4$), a mineral commonly used for rock dating applications. However, the coincidence between the distribution of the trace elements and the CL image does not always allow us to conclude that the detected impurities are the activators of the luminescence emission. The CL emission depends not only on the presence of doping elements but on all deviation from stoichiometry as discussed by Onasch and Vennedanne (1995). In addition to elemental composition variations, structural defects must also be considered for a reliable interpretation of the contrasts of CL images and CL emission spectra.

It is the purpose of this paper to investigate the possible use of CL imaging for the study of the localization and the spatial distribution of doping elements added into synthetic zircon crystals prepared by the flux method (Cesbron *et al.*, 1995). Each of the sets of crystals was doped with a single rare-earth element (REE) in the form of $(REE)^{3+}$ ions, with addition of phosphorous into the flux in order to maintain the electric charge equilibrium. Two observation modes of the luminescent properties of the crystals were used: (1) color photographs recorded through an optical microscope equipped with a cold cathode electron gun, and (2) black and white CL images obtained using a SEM equipped with a CL spectrometer. With the SEM, spectrally non-decomposed images and selected wavelength images were

obtained. As shown in the previous paper (Cesbron *et al.*, 1995), the CL emission spectra of the REE-doped zircons consist of narrow peaks characteristic of the doping REE ions and a broad polychromatic emission resulting from structural defects and additional impurities different from the REE ions. Based on the shape of the CL emission spectra of the synthetic REE-doped zircons reported by Cesbron *et al.* (1995), two groups of crystals with different CL properties can be expected: (1) Crystals exhibiting several sharp intense CL peaks occurring within the visible part of the spectrum with a weak ultra-violet (UV)-blue intrinsic emission. For such spectra, the contrasts of the CL images are expected to be dominated by the intensity of the CL emission being characteristic for the corresponding REE doping ion. (2) Zircons consisting of crystals exhibiting a maximum CL intensity corresponding to the intrinsic emission within the UV-blue region with some weak narrow peaks occurring in the visible part of the spectrum. For these crystals (exhibiting a blue CL hue), the contrasts of CL images are expected to be very complex due to the simultaneous contribution of the luminescent ions and structural defects in the CL emission mechanisms.

Spatially resolved X-ray spectrometry with the electron probe micro-analyzer (EPMA) and with the micro-PIXE (particle induced X-ray emission) was used for comparing the spatial distribution of the impurities present in the synthetic zircons with the contrasts of the CL images. It will be shown that based on chemical analysis alone, it is not possible to conclude the existence of only one relationship between the distribution of all detected impurities and the contrasts of CL images (non-spectrally decomposed and selected wavelength images corresponding to the REE^{3+} CL emission). It will be illustrated that surface and bulk electrostatic charging phenomena resulting from the presence of all impurities must be considered rather than the qualitative and quantitative chemical analyses alone. The contribution of the host lattice CL emission to the intensity of a characteristic CL emission of the REE^{3+} ions will be discussed by referring to the role of strong electrical fields resulting from charge trapping mechanisms on structural defects. For this purpose, charging effects will be illustrated by studying the changes of the Duane-Hunt limit measured on X-ray energy dispersive spectra (EDS) as a function of the excitation conditions. In order to express the intensity of a characteristic CL emission as a function of the concentration of the corresponding REE activator, the different mechanisms of generation of CL photons will be considered: (1) the direct excitation of the REE^{3+} ion (charge conversion mechanism); and (2) the excitation of the activator by the intrinsic emission according to a radiative or a non-radiative process (energy transfer mechanism).

Materials and Methods

An optical CL microscope equipped with a cold cathode electron gun was first used to verify the homogeneity of incorporation of the doping elements. Figure 1 shows the CL images for an undoped zircon and for Ce, Nd, Gd, Eu, Tm, Dy and Tb doped zircons.

In a first set of experiments, the synthetic zircons were first cleaned with hydrochloric acid and then, ultrasonically cleaned with distilled water before direct CL observation and photographic recording. The observed CL emission was found to be homogeneous in color and intensity at the surface of the unpolished surfaces of Dy and Tb doped zircons (Fig. 1). In a second experiment, the zircons were embedded in plastic and polished using abrasives of decreasing grain size. The resulting polished surfaces are obviously a few hundreds of micrometers below the original manufactured surfaces. After polishing, all crystals exhibited variations of the observed CL hue as a function of the incorporated REE activator and, for a given REE ion, exhibited local changes in intensity of the CL emission as shown in Figure 1.

CL spectroscopy and microscopy were also performed using a SEM equipped with a CL spectrometer as previously described (Cesbron *et al.*, 1995). Non-spectrally decomposed (polychromatic) images were obtained when the slit of the CL spectrometer was opened so that the entire wavelength domain ranging from 200 to 900 nm was used for imaging. Monochromatic CL images were also obtained for selected wavelengths corresponding to the characteristic CL peaks of the REE activator ions or to the intrinsic emission of the host crystal lattice.

All CL measurements were carried out at **room temperature**. With the CL optical microscope the synthetic zircons were observed without surface coating. For CL studies with the SEM, all specimens were polished and coated with a 20 nm thick carbon film. The contrasts of the CL images were correlated with the distribution of impurities analyzed by means of X-ray spectrometry induced either by electron (EPMA) and or proton bombardment (PIXE). The spatial distribution of the REE and phosphorous added to the synthetic zircons was studied by X-ray mapping on EPMA. The digital X-ray maps were obtained by stepping the specimen under the electron beam. This procedure avoids focusing defects when large areas are analyzed. The images contain 512 x 512 pixels. The zircon crystals have average dimensions of about one millimeter so that the lateral resolution on the X-ray maps is only about 20 μm which is insufficient to reveal the major structures shown on the color CL image. Furthermore, the X-ray maps reflect the spatial variations of the total X-ray peak, i.e.,

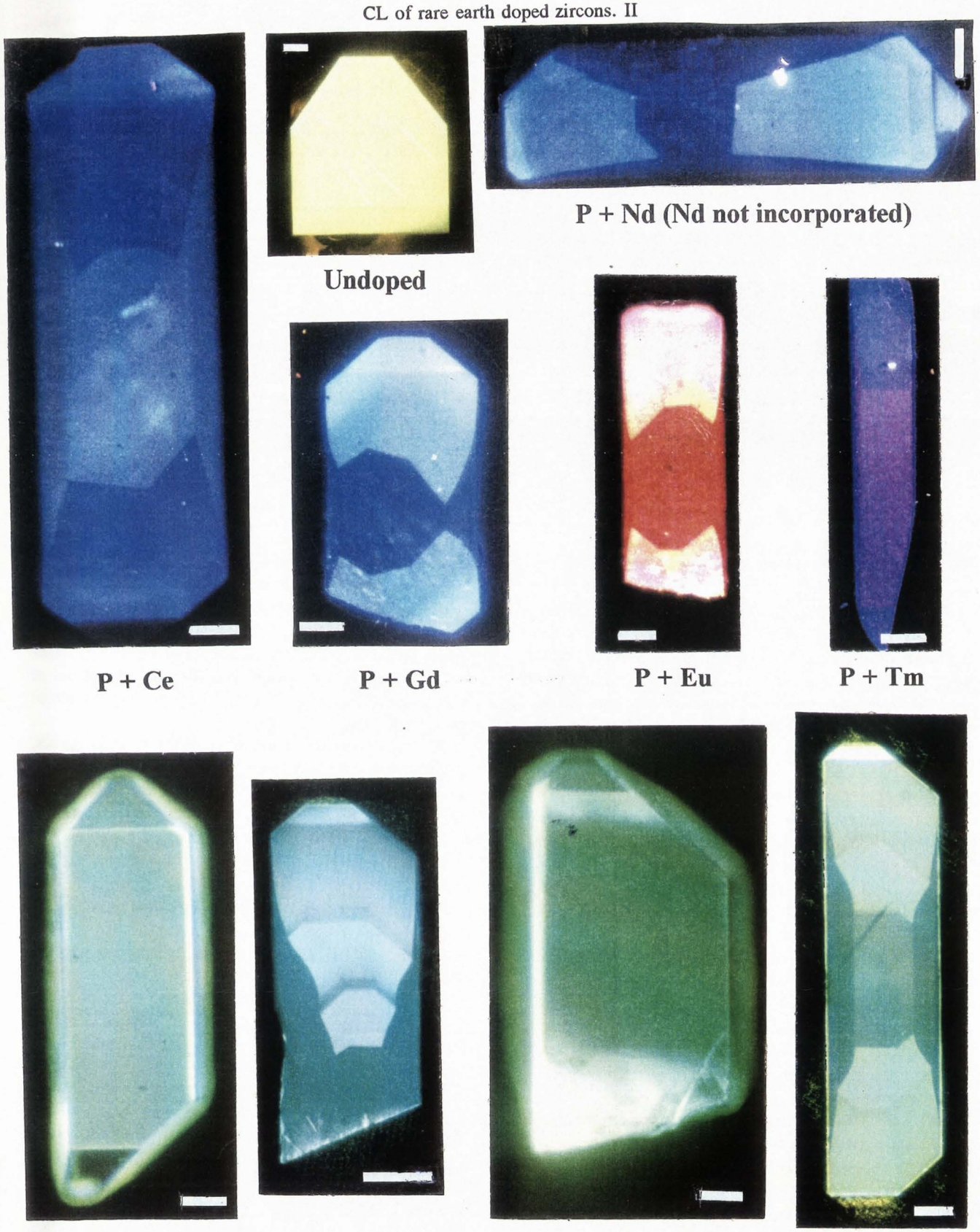

Figure 1. CL microscopy (using the optical CL microscope) of some REE-doped synthetic zircons. Except when specified, the zircons are prepared as polished sections. Bars = 200 μm.

Table 1. REE and P elemental concentrations within areas of the synthetic doped zircons exhibiting low and high CL brightness on the color CL images in Figure 1.

REE Doping Element	Dy	Tb	Eu	Nd	Gd	Ce
CL Hue	Blue-green	Yellow-green	Orange	Blue	Blue	Blue
Lower CL Brightness	Dy ~ 0.15%	Tb ~ 0.1%	Eu ~ 300 ppm	Nd ≤ LOD*	Gd ~ 400 ppm	800 ≤ Ce ≤ 200 ppm
	P ~ 0.5%	P ~ 0.25%	P ~ 0.15%	P ~ 0.2%	P ~ 0.15%	0.1% ≤ P ≤ 0.25%
Higher CL Brightness	Dy ~ 0.3%	Tb ~ 0.35%	Eu ~ 1000 ppm	Nd ≤ LOD*	Gd ~ 1250 ppm	Ce ≤ LOD*
	0.5% ≤ P ≤ 0.7%	0.1% ≤ P 0.2%	0.1% ≤ P ≤ 0.2%	P ~ 0.1%	0.1% ≤ P ≤ 0.25%	P ~ 0.15%

*The limits of detection (LOD) were derived from line profiles and point analyses using micro-PIXE (see text).

the intensities of the analyzed X-ray lines and the underlying continuous X-ray emission measured with a 0.1 second counting time per step. Only X-ray intensity variations greater than several tens of percent can lead to observable contrasts on the X-ray maps. To improve the sensitivity of detection, 100 quantitative analyses were performed step by step with 30 second counting time for the X-ray intensities measured at the peak maximum and on each side of the peak (continuous emission). The analyzed points were distributed with a constant step along a direction crossing the longest dimension of the crystals. These experimental data were corrected for matrix effects and spectral interferences which were neglected during the X-ray mapping technique. The P Kα peak overlaps the Zr Mζ peak. By analyzing a P free synthetic zircon, the Zr Mζ peak intensity was found to be equivalent to 1480 ppm of P. All point analyses along the line scans were corrected for this 1480 ppm value. On the continuous X-ray emission of a target, the Duane-Hunt limit is the cut-off energy of the generated X-ray photons indicating the maximum kinetic energy of the incident electrons striking the specimen surface. For measuring the Duane-Hunt limit, a JEOL 5400-LV SEM equipped with a Kevex Sigma EDS detector was used.

For energy dispersive X-ray spectrometry induced by proton irradiation, two micro-PIXE equipments were used: (1) In one of them, installed at the CNRS-CERI laboratory in Orléans, France, the size of the proton beam impinging the specimen surface was 30 μm x 40 μm. (2) The equipment at the Nuclear Physics Department at the University of Lund, Sweden, employs a beam of 2 μm diameter; 64 points by 64 points X-ray maps were obtained for all detected trace elements. For each analyzed element, a line profile was extracted from the X-ray image, and each of the 64 point analyses distributed along the scan was corrected for matrix effect. For each data point, the detection limit was also calculated. The charge accumulated per pixel along the line scan was about 1 nC for high atomic number REE (Lu) and about 7 nC for low atomic number REE (Ce). Under these acquisition conditions, the detection limit at each analyzed point was about 80 ppm for Lu and about 150 ppm for Ce.

By increasing the counting time for specific points, the detection limit can reach ppm level. The complementarity of the EPMA and micro-PIXE for the localization of REE at trace levels in zircons has been illustrated by Rouer *et al.* (1995) and Rémond *et al.* (1995).

Spatially resolved X-ray data showed that Hf (in amounts from 200 to 300 ppm), Mn, Cr and Fe (in amounts of 30 to 50 ppm) were present but were homogeneously distributed within all synthetic zircons. On the contrary, the REE and P ions analyzed with both the EPMA and the micro-PIXE exhibited heterogeneous spatial distribution revealing features similar to those shown on the CL images of the REE-doped zircons crystals. The average REE and P concentrations as a function of the CL brightness observed on the color CL images are summarized in Table 1.

Relationship Between the Contrasts of CL Images and the Concentration of the Doping Elements

Dy-doped and Tb-doped zircons

The blue-green and yellow-green CL colors of the Dy and Tb doped zircons respectively (Fig. 1) mainly originate from the characteristic monochromatic CL lines of each specific REE doping ions with a small contribution of the intrinsic emission band. This statement is

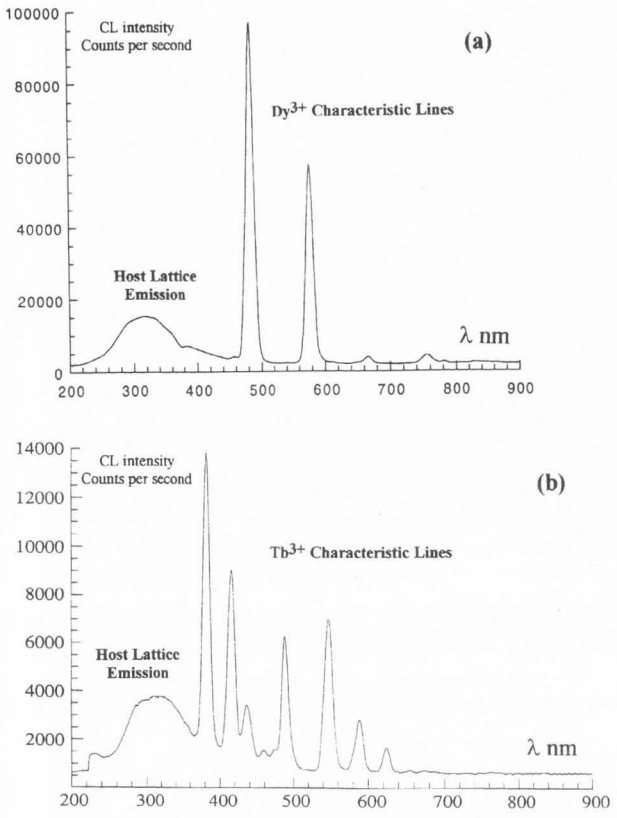

Figure 2. CL emission spectra measured (at room temperature) at the surface of (a) a Dy-doped and (b) a Tb-doped synthetic zircons. The spectra are not corrected for the response function of the CL spectrometer.

---

supported by the spectra in Figures 2a and 2b for Dy-doped and Tb-doped crystals, respectively. For each crystal, the shape of the CL emission spectra remained independent of the analyzed areas, only the intensities of the peaks changed when measured at several locations on the surface. The CL spectrum of the Dy-doped zircon (Fig. 2a) exhibits two intense narrow peak centered near 485 nm (blue-green) and 580 nm (yellow-green), while, the intrinsic emission occurring in the UV-blue part is very low and probably does not significantly contribute to the observed CL hue owing to the spectral response function of the optical CL microscope (as discussed later). Similarly, the yellow-green CL hue for the Tb-doped zircon (Fig. 1) results from the mixture of monochromatic colors associated with the characteristic emission peaks (Fig. 2b) occurring near 490 nm (blue-green) and 550 nm (yellow-green) with other emissions of lower intensities at longer wavelengths. The peak centered near 385 nm measured on the CL spectrum probably contributes to a minor extent to the observed

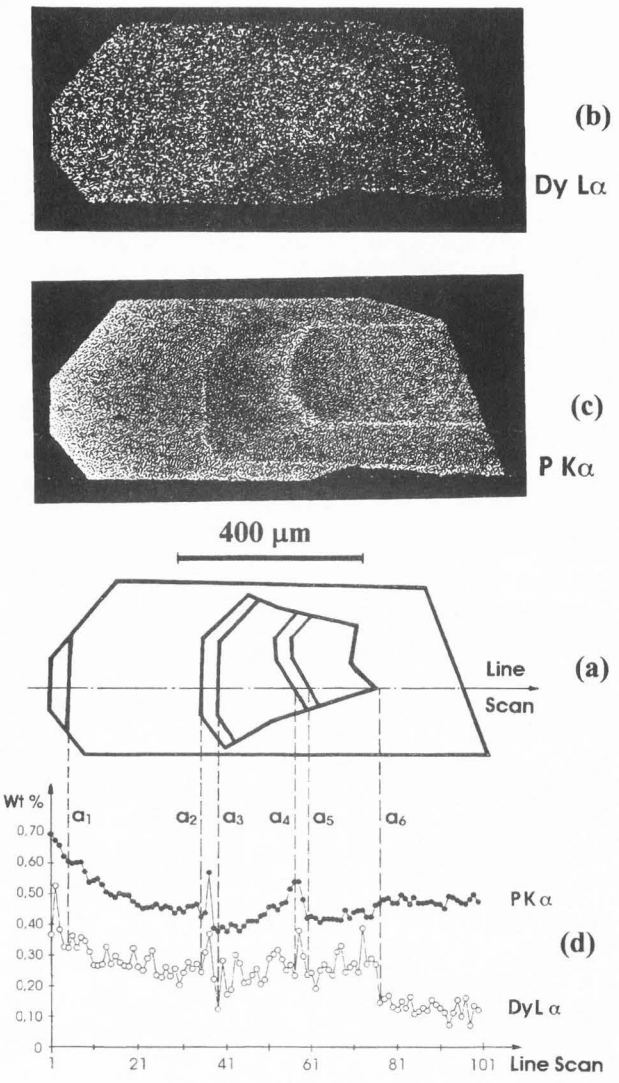

Figure 3. Polished Dy-doped zircon. (a) Schematic illustration of the areas exhibiting CL intensity variations of the blue-green CL hue on the color image in Figure 1. EPMA X-ray maps for (b) Dy Lα and (c) P Kα. (d) Dy Lα and P Kα EPMA quantitative line scans along the direction marked on the schematic view (a).

---

color of the CL emission.

For the Dy-doped zircon, several areas can be distinguished by the change in brightness of the blue-green emission (Fig. 1). The outer area, lying between the edge of the crystal and the line labelled a_1 (on the schematic view of the crystal in Figure 3a) exhibits the highest CL intensity. The areas [a_1, a_2], [a_3, a_4] and [a_5, a_6] are separated by thin interfaces [a_2, a_3] and [a_4, a_5] exhibiting a lower CL intensity than that of the adjacent

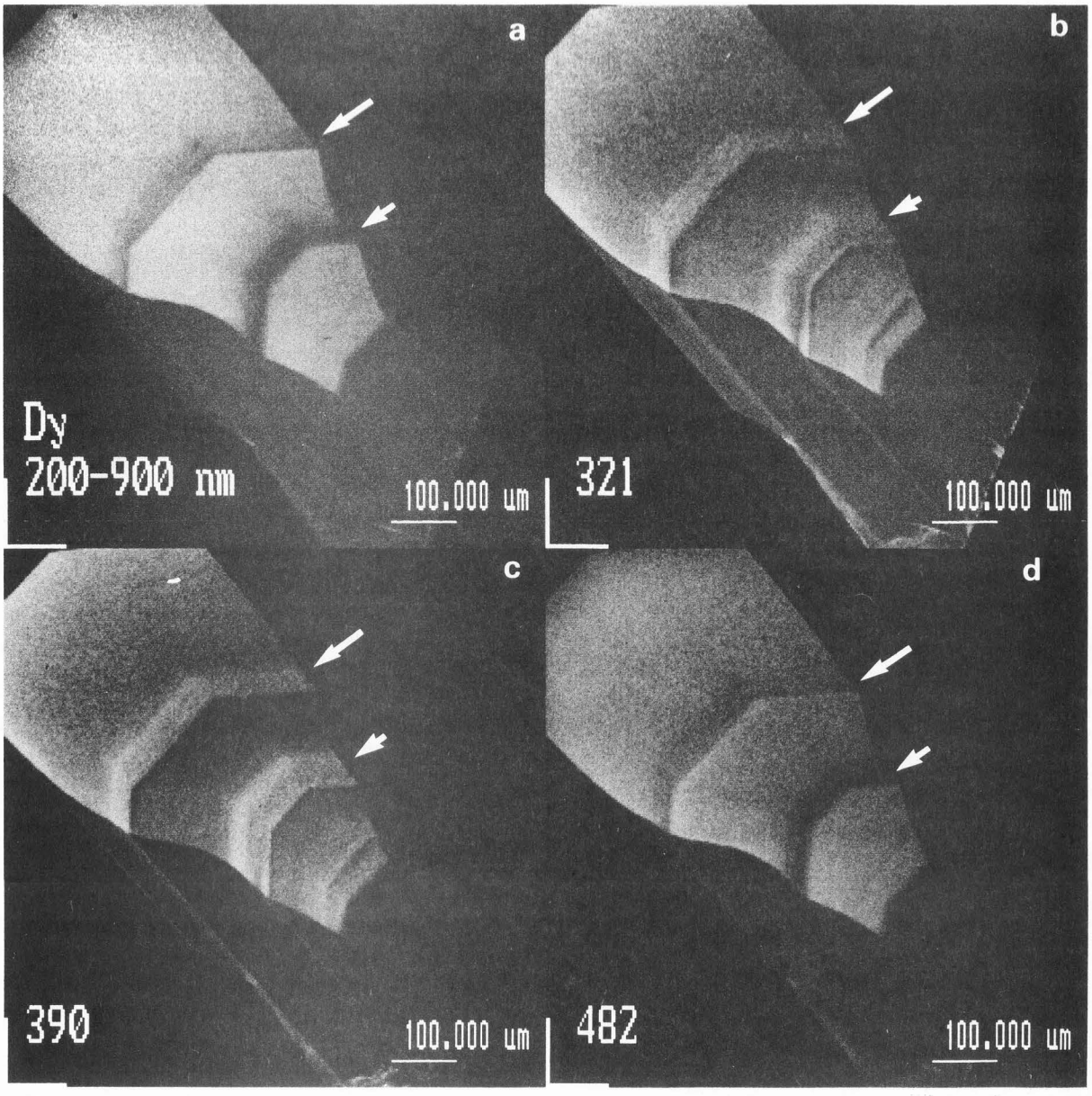

Figure 4. Polished Dy-doped zircon. The CL images were recorded using a SEM equipped with a CL spectrometer. **(a)** Non-spectrally resolved image corresponding to the total wavelength domain extending from 200 nm to 900 nm; selected wavelength images at λ = 321 nm (b), and at λ = 390 nm (c) associated with the intrinsic CL emission; and at λ = 482 nm (d) corresponding to a characteristic emission line of the Dy^{3+} ions. Note contrast reversals at areas marked by arrows.

areas. The CL intensity then decreases within the outer area lying at the right hand side of the line marked a_6 in Figure 3a.

As shown on the EPMA X-ray maps and the quantitative line scans (Figs. 3b and 3c), the area exhibiting the lower CL brightness corresponds to the lower Dy concentration and the higher P concentration which may suggest that P acts as a killer of CL emission. However, within the areas [a_1, a_2], [a_3, a_4] and [a_5, a_6], both the Dy and P concentrations show similar variations (X-ray line scans in Fig. 3d). These line scans also showed a simultaneous sharp increase of the Dy and P concentrations at the growth interfaces [a_2, a_3] and [a_4, a_5]. **Because these narrow interfaces have lower CL intensities than those of the adjacent areas, it is not possible to conclude that there exists a unique relation between the brightness of the CL hue and the weight concentration of the impurities.** The variations in the

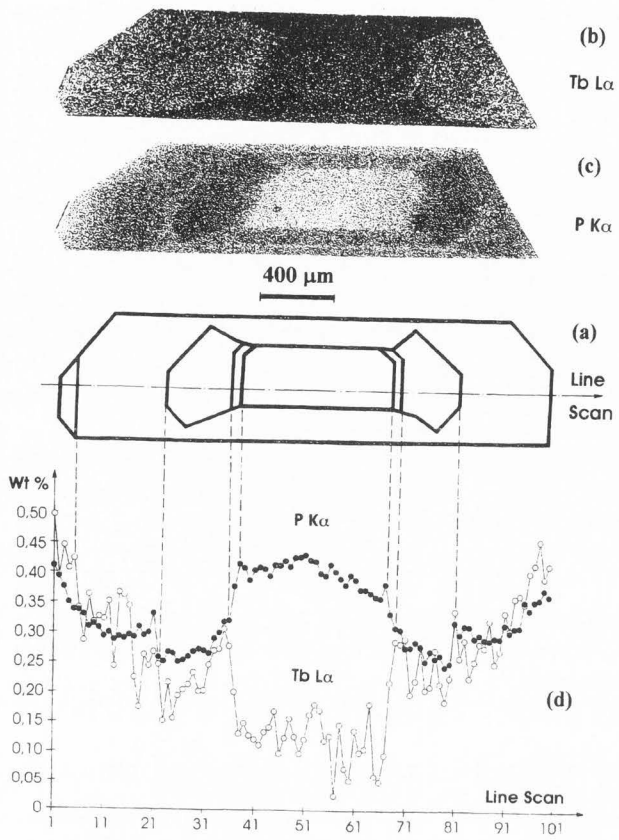

Figure 5. Polished Tb-doped zircon. (a) Schematic illustration of the areas exhibiting CL intensity variations of the yellow-green CL hue in Figure 1. (b) Tb Lα and (c) P Kα X-ray maps (by EPMA), and, (d) Tb Lα and P Kα EPMA quantitative line scans along the direction marked on the schematic view of the crystal (a).

---

intensity of the CL emission observed at the apex of the crystals on the color images (area ranging between the edge of the crystal and the a_1 line marked in Fig. 3a) more probably results from a geometrical effect due to the presence of pyramidal faces at the apex of the crystals rather than from a chemical effect. This statement is supported by the fact that the concentrations of both the Dy and P elements exhibit a continuous decrease from the apex to the center of the crystal while the areas revealed by changes in the CL intensity exhibit sharp contours. The thickness of the crystal near the rims being thinner than that at the core, the CL photons generated near the crystal edges are submitted to less absorption by the matrix than those generated within the core of the crystal. Simultaneously, the change in the orientation of the crystallographic planes resulting from the existence of pyramidal faces at the ends of the crystals

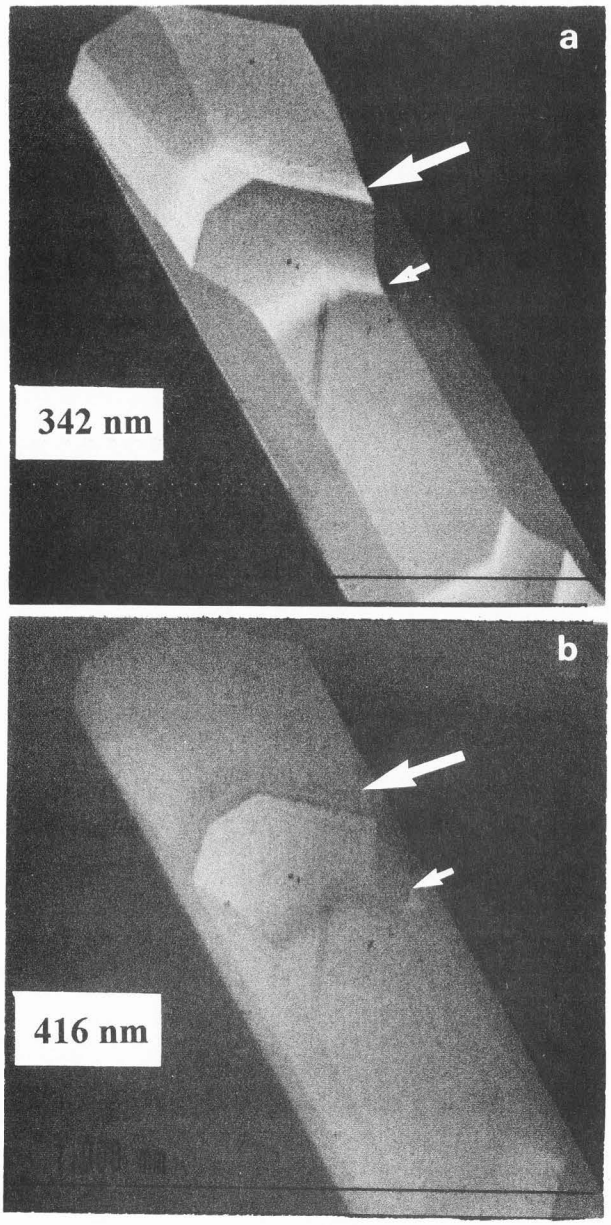

Figure 6. Spectrally resolved CL images recorded at the surface of a polished Tb-doped zircon at (a) λ = 342 nm associated with the intrinsic CL emission and (b) λ = 416 nm corresponding to a characteristic emission line of the Tb^{3+} ions.

---

may lead to internal reflection of the CL beams within the crystal. Both effects, absorption and edge phenomena, may contribute to local changes of the CL intensity measured at the surface of a crystal having homogeneous internal CL properties.

The polychromatic CL image corresponding to the 200-900 nm wavelength interval is shown in Figure 4

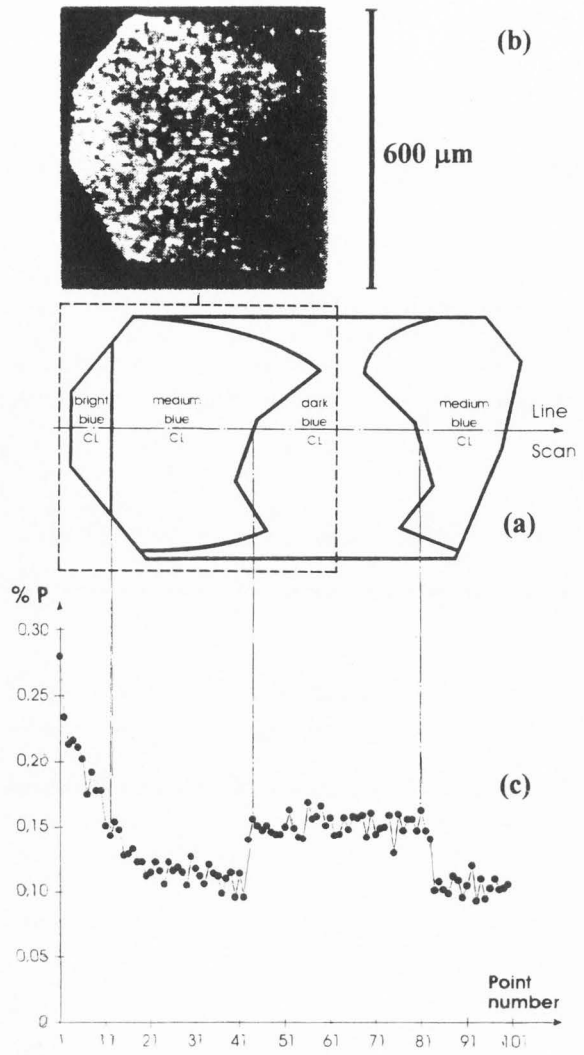

Figure 7. Polished Gd-doped zircon. (a) Schematic illustration of the areas exhibiting CL intensity variations of the blue CL hue on the color image in Figure 1. (b) Micro-PIXE Gd Lα map and (c) P Kα EPMA quantitative line scan along the direction marked on the schematic view of the crystal.

---

for the Dy-doped zircon. The contrasts of this non-spectrally decomposed CL image are similar to those shown on the monochromatic image at λ = 482 nm in Figure 4 corresponding to a characteristic emission line of the Dy^{3+} ions. This result confirms that the variations in brightness in Figure 1 are dominated by the intensities of the monochromatic lines associated with the REE doping ions and consequently, illustrate the spatial distribution of the Dy^{3+} ions. The variations of the CL intensity on the image associated with the Dy characteristic CL emission correspond to variations of the concentration of the REE ions. Additional features are revealed by the CL images at λ = 321 and 390 nm (Fig. 4) corresponding to the intrinsic CL emission; also note contrast reversal in some areas (marked by arrows in Fig. 4). This reversal in contrast is particularly noticeable at narrow interfaces (marked [a_2, a_3] and [a_4, a_5] in Fig. 3) between two adjacent growth areas exhibiting different CL intensities. These inter-growth areas correspond to an increase of both the Dy and P concentrations (see line scans in Fig. 3) with respect to the concentrations of these elements within the adjacent crystallites. The reverse contrasts within the [a_2, a_3] and [a_4, a_5] areas as a function of the selected wavelengths corresponding to a characteristic Dy^{3+} CL line and for the intrinsic emission band indicates that the contrasts of the CL images cannot be only explained on the basis of changes in elemental composition of the specimen. The same results are obtained for the Tb-doped zircon (Figs. 5 and 6): the areas exhibiting the highest CL brightness correspond to the highest REE elemental concentrations and that the decrease in CL intensity corresponds to a decrease of the REE content with a simultaneous increase of the P concentration. Again, contrast reversals at growth boundaries, as shown by comparing CL images at wavelengths characteristic of the Tb^{3+} ions and of the intrinsic emission band, are present (Fig. 6).

Gd-doped, Eu-doped, P-doped and undoped zircons

The role of P as a possible killer of the CL intensity when combined with a specific REE ion was noted for zircons doped with Eu (results not shown) and Gd (Fig. 7). As shown in Figure 1, the cores of the crystals exhibit a darker blue CL (Gd-doped zircon) or a darker orange CL (Eu-doped zircon) than the CL emission at the ends of the crystals. The micro-PIXE X-ray map in Figure 7 (for Gd-doped zircon), shows that the brighter CL areas correspond to an increased REE concentration, as compared to the concentration of that dopant at the core of the crystal (emitting a dark blue CL emission, Fig. 1). The P Kα EPMA line scan (Fig. 7), along the length of the Gd-doped crystal showed a continuous decrease of the P concentration when the electron beam was moved from the edge to the core of the crystals before reaching a plateau value within the core of the crystals. The same variations were observed for the case of the Eu-doped zircon indicating a positive correlation between the CL brightness and the concentration of Gd or Eu doping ions. However, the role of P is again ambiguous. Although the REE ion concentrations decrease within the areas of lower intensity, the concomitant increase of the P concentration suggests that this element could act as a killer of luminescence. The edge of the crystal exhibits a very intense bright blue CL corresponding to a simultaneous decrease of the Gd and P concentrations. These variations are in contradiction

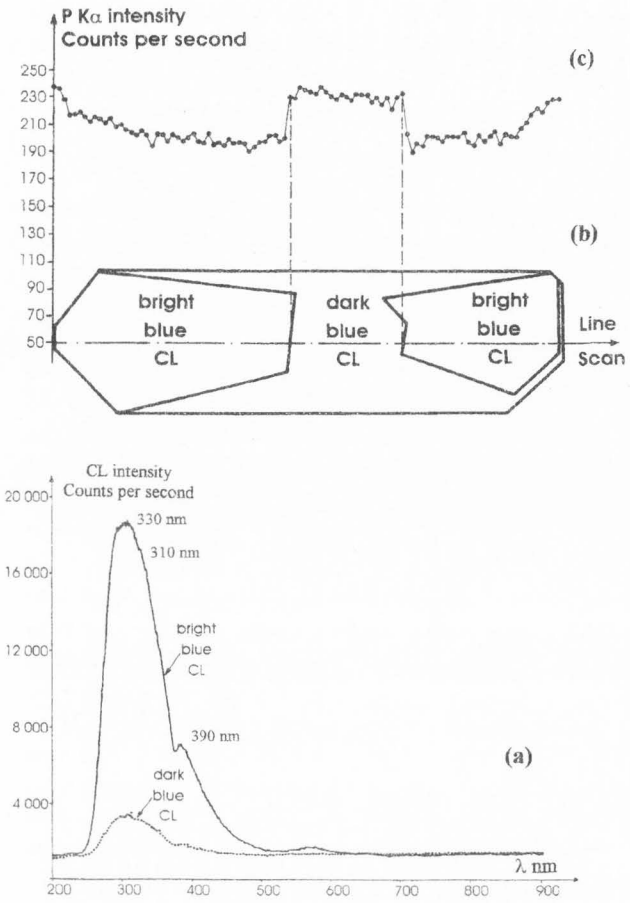

Figure 8. Polished P-doped zircon. (a) CL emission spectra measured at the surface of the areas emitting a dark and a bright blue hue; (b) schematic illustration of the areas exhibiting CL intensity variations of the blue CL hue on the color image in Figure 1 and (c) P Kα EPMA quantitative line scan along the direction marked on the schematic (b).

---

with the possible role of P as a killer of luminescence but, as previously reported for the Dy-doped crystal, a geometrical effect may be responsible for the very high CL intensity at the outer edge of the crystal and the role of P remains ambiguous.

As shown in Figure 1, the crystal labelled Nd-doped zircon is characterized by a blue CL emission. As already mentioned in the previous paper (Cesbron *et al.*, 1995), the Nd doping ions were not incorporated into this particular zircon with a sufficient enough concentration for inducing a characteristic emission of the Nd ions and only P was actually incorporated as a doping impurity. Consistent with CL spectrometry, which did not reveal CL characteristic lines of the Nd ions, micro-PIXE did not detect the presence of Nd (detection limits:

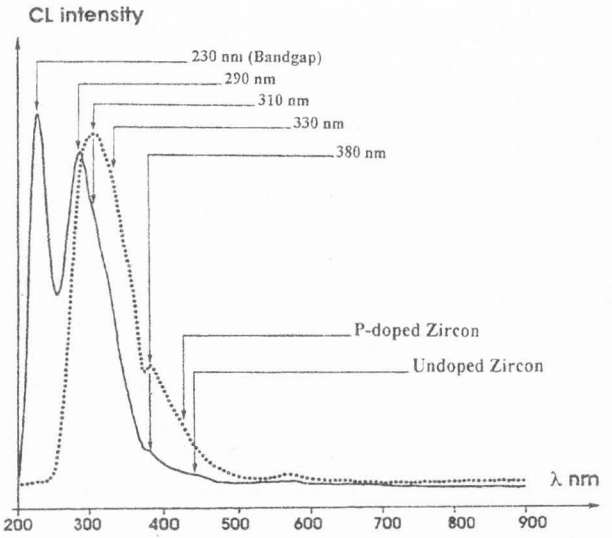

Figure 9. Effect of the addition of P on the shape of the intrinsic CL emission of zircons. Dotted curve: P-doped, and solid curve: undoped zircons.

---

220 ppm for the line scan and 6 ppm for point analysis, as discussed by Rouer *et al.*, 1995). For these reasons, this crystal will be referred in the following as **P-doped** zircon. Only broad intrinsic CL emission bands in the UV and blue part were measured at the surfaces emitting a dark or a bright blue CL emission (Fig. 8a): the intense emission band maximizes near 310 nm with a shoulder at 330 nm, and a second band of lower intensity has its maximum near 380 nm. The area at the center of the crystal exhibiting the dark blue CL emission (Fig. 8b), i.e., the lower UV-blue CL host lattice emission, corresponds to an increase of the P concentration (see P Kα EPMA line scan in Fig. 8c).

An undoped synthetic zircon was prepared without any addition of REE and P. This crystal exhibits a yellow hue (see bottom left micrograph in Fig. 1). The CL emission spectrum, from this undoped crystal, shows an intense peak centered at 230 nm, a second peak centered at 290 nm with a shoulder at 310 nm, and a third weak asymmetrical band at 380 nm (Fig. 9). The emission band centered at 230 nm disappears when P^{5+} ions are added as a doping element in the synthetic crystal as shown by the solid curve in Figure 9. Also, the intensities of the peaks within the UV region change when P is present as an impurity in the zircon. More particularly, the intensities of the peaks at 310 nm, 330 nm and 380 nm relative to the intensity of the peak at 290 nm are much lower for the undoped crystal than for the P-doped zircon. These emissions result in a high integrated CL intensity within the UV-blue region for the P-doped zircon leading to the blue CL hue observed on the color image for Nd-doped zircon in Figure 1. There is

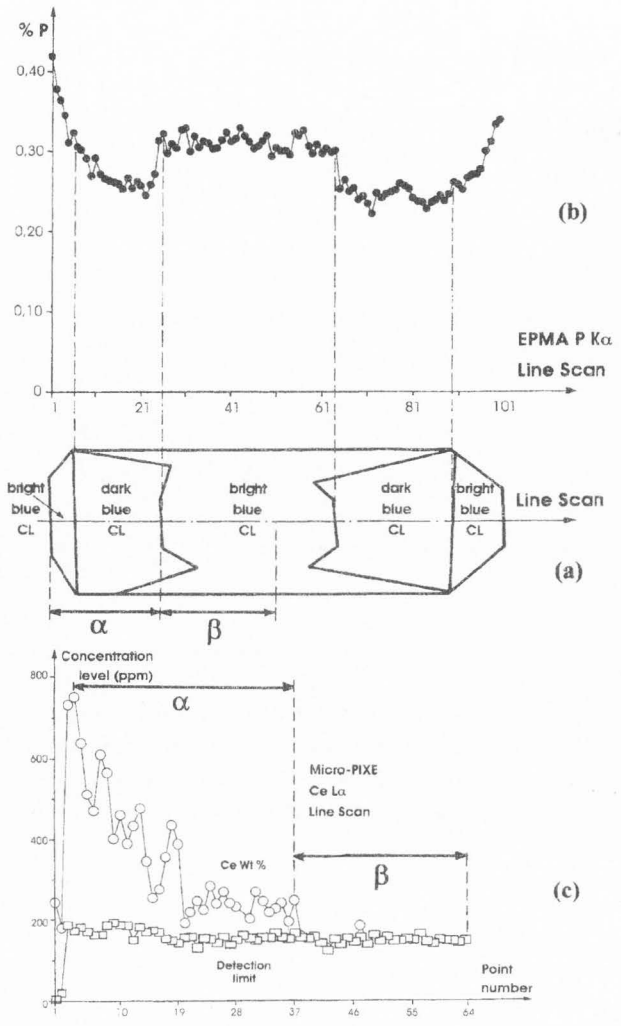

Figure 10. Polished Ce-doped zircon. (a) Schematic illustration of the areas exhibiting CL intensity variations of the blue CL hue in Figure 1. (b) EPMA P Kα quantitative line scans along the direction marked on the schematic view (a) and (c) micro-PIXE Ce Lα line scan from the end to the center of the crystal.

---

no evidence for an emission band within the yellow part of the spectrum in Figure 9 for the case of the undoped zircon. The spectrometer attached to the SEM and the CL optical microscope the have different transmission efficiency as a function of wavelength. The CL intensity measured in the UV-blue region on the spectra with the SEM CL equipment is not the same as that measured with the CL optical microscope. Only photons with wavelengths above a threshold resulting from instrumental factors will contribute to the contrast of the color CL images; this is similar to the situation for the yellow CL hue of the undoped zircon as shown in Figure 1. Neglecting the response function of the equipments makes it impossible to compare CL images of different crystals and may also lead to false interpretation of contrasts in CL images observed at the surface of a single crystal (illustrated below for the Ce-doped zircon).

Ce-doped and Tm-doped zircons

As shown in Figure 1, the Ce-doped crystal also exhibits a blue CL hue with local changes in its brightness. The micro-PIXE line scan in Figure 10 shows that the Ce concentration followed a continuous decrease from about 800 ppm at the outer edge of the crystal to about 200 ppm at the dark/bright CL boundary (a value close to the detection limit of about 150 ppm found from the line scan). From the line scan, we conclude that the amount of Ce present within the center of the Ce-doped zircon (exhibiting the bright blue CL emission in Fig. 1) was below its limit of detection. P concentration continuously decreased before reaching a plateau when the beam was moved from the edge of the crystal to its center exhibiting the brighter blue CL hue (EPMA line scan in Fig. 10c). The variations of the P concentrations within the Ce-doped zircon are similar to those observed for other crystals also exhibiting a blue CL hue, however, **the P concentration plateau value at the core of the crystal corresponds to the darker blue hue area within the Gd-doped crystal (Fig. 7), while, for the Ce-doped zircon, the P plateau is associated with the brighter blue CL emission.**

Figure 11 shows the black and white CL images for Ce-doped zircon. The non-spectrally decomposed image (200-900 nm) (Fig. 11, top left) shows reversed contrasts compared with those observed on the color image (Fig. 1), i.e., a higher CL intensity in the central area on the non-spectrally resolved black and white image than that occurring at the ends of the zircon crystal, while on the color image in Figure 1, the center of the crystal exhibited a brighter blue hue than the edges of the crystal. The slight variations in intensities observed near the edges of the crystal again probably resulted from a crystal thickness effect as previously mentioned. The same contrasts, as those of the non-spectrally decomposed image, are also observed on the monochromatic CL images corresponding to the wavelengths selected at $\lambda = 335$ and $\lambda = 395$ nm. The contrast is reversed when the wavelength used for imaging was set at $\lambda = 450$ nm, i.e., at 450 nm, the ends appear darker than the core of the crystal.

In order to explain the contrast changes as a function of recording modes [color image with a cold cathode electron gun (Fig. 1) versus polychromatic image with the SEM and at selected wavelengths (Fig. 11)], CL emission spectra were measured at the end and at the center of the Ce-doped zircon (Fig. 12). For both areas,

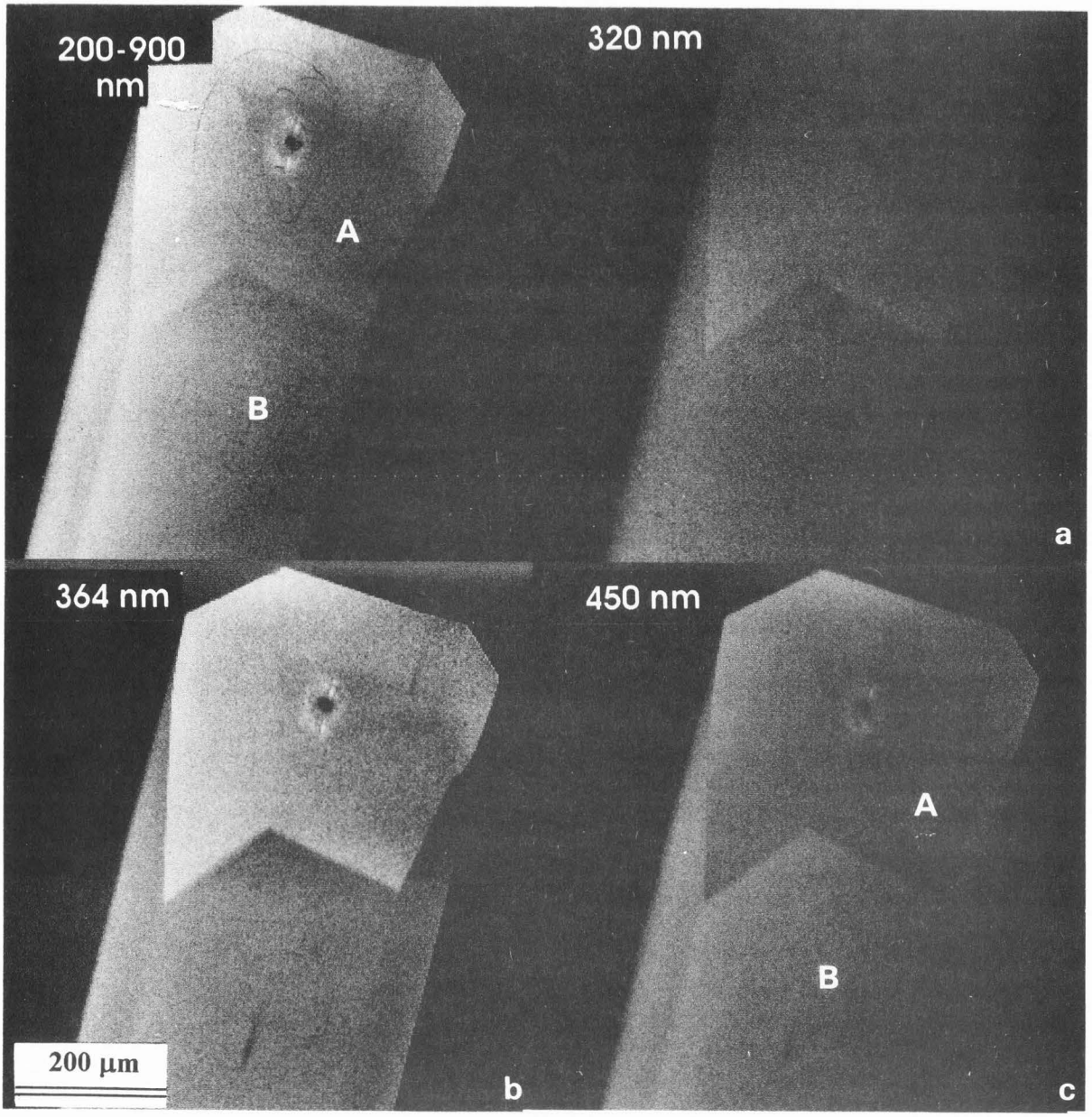

Figure 11 (above). Polychromatic and selected wavelength CL images for a polished Ce-doped zircon. The images a, b and c correspond to the wavelengths marked on the CL spectra in Figure 12. Note the reversal of contrasts in the image at λ = 450 nm. The dark spot identifies the location of X-ray point analysis.

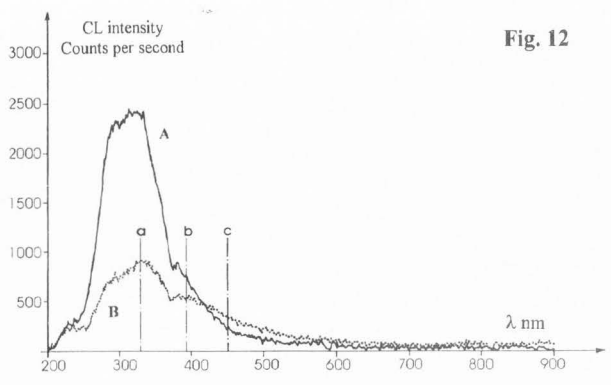

Fig. 12

Figure 12 (at left). CL emission spectra measured at the end (location A in Fig. 11) and the center (location B in Fig. 11) of the Ce-doped zircon.

the CL photon distribution consists of broad emission bands within the UV and blue part of the visible spectrum. A very weak band maximizes at 230 nm, two peaks with amplitude in the same order of magnitude are centered at about 290 nm and 335 nm, and a fourth band extends from about 380 nm with a maximum near 395 nm before slowly decreasing within the visible part of the spectrum leading to an asymmetrical shape of the emission band. As shown in Figure 12, for wavelengths between 200 nm and 430 nm, the CL intensity measured at the center of the crystal remains lower than that measured at the end of the zircon. For wavelengths greater than 430 nm, the opposite situation is observed. The contrast reversal between the center and the ends of the Ce-doped zircon shown on the color (Fig. 1) and the black and white (Fig. 11) images may be possibly due to a difference in the response function of the two equipments. For the color photographs (Fig. 1), the specimen is isolated from the air by a glass plate which does not permit the transmission of the UV part of the spectrum. The glass plate is rapidly contaminated by polymerized hydrocarbon species arising from the residual air in the specimen chamber as well as the contaminated specimen surface. Rapidly, the glass plate turns to a brown color during the irradiation and this contaminant film will increase the absorption of the short wavelength CL photons. In case of the optical CL microscope, if we reasonably postulate that the CL photons with wavelengths lower than about 400 nm are not transmitted, the integrated CL intensity for wavelengths greater than 400 nm will be higher for measurements at the center than at the end of the crystal. Consequently, the brightness of the blue hue on the color image will be higher at the center than that at the ends of the specimen as was observed in Figure 1. All CL photons with wavelengths in the 200-900 nm domain participate to the polychromatic CL image obtained with the SEM/CL spectrometer attachment. From the spectra in Figure 12, the integrated CL intensity within the 200-900 nm domain is higher when measured at the ends of the crystal than for areas located in the center of the Ce-doped zircon; this leads to the contrast observed on the polychromatic CL image in Figure 12. For all wavelengths lower than 430 nm, the CL intensity increases when the beam is moved from the center to a location close to the end of the crystal and the contrasts of the monochromatic images at 335 nm and 395 nm are identical to those observed on the polychromatic image. For wavelengths greater than about 430 nm, the CL intensities show opposite variations as a function of the beam location and monochromatic CL images for selected wavelengths greater than this threshold exhibit a decrease in brightness at the ends of the crystal compared with that observed at its center.

The CL emission spectrum for the Ce-doped zircon (Fig. 11) does not show narrow peaks being characteristic of the Ce^{3+} ions and only emission bands are observed within the wavelength interval containing the UV-blue intrinsic emission (being characteristic of the host crystal lattice). The emission bands near 290 nm, 330 nm and 390 nm are very similar to the intrinsic emission bands for the case of the undoped and the P-doped crystals (Fig. 9). Chapoulie *et al.* (1995) reported a CL emission band at 370 nm in Ce-doped calcite crystals. This value is close to the peak at about 390 nm on the emission spectrum of the Ce-doped zircon (Fig. 12). Thus, it is difficult to separate with certainty the part of the spectrum related with the Ce luminescent activator from the contribution of the crystal lattice imperfection. Consequently, it is not possible to identify on the CL images (even on selected wavelength images) the areas in which Ce was incorporated as a doping element.

The presence of P modifies both the intrinsic and the REE characteristic emission intensities as illustrated for the Tm-doped zircon (Fig. 13). In Figure 1, the ends of the Tm-doped crystal exhibit a blue color and the core of the crystal shows a purple hue. On the non-spectrally resolved CL image with the SEM shown in Figure 13, the edges of the crystal (blue color) appear darker than the center of the crystal (purple color). For both areas, the ends and the core of the Tm-doped zircon, the CL emission spectra in Figure 13 show narrow emission peaks which may be due to the presence of the doping Tm ions. The intensity of these peaks are higher when the spectrum is obtained from the center (purple CL) than at the edges of the crystal (blue CL). These variations suggest that a higher concentration of Tm ions should be present in the core of the crystal while the opposite situation is encountered at the crystal ends as illustrated by the EPMA line scan in Figure 13. On the contrary, EPMA data did not reveal significant variations of the P concentration along the same line scan. As shown in Figure 13, a broad intrinsic band in the UV-blue region is observed when the CL spectrum is recorded at the ends of the Tm-doped crystal (blue CL color) while a much lower intrinsic contribution is observed at the center of the crystal (purple color). This result indicates that the edges have more intrinsic defects than the center of the Tm-doped zircon. In addition, the characteristic Tm emission occurring near 350 nm overlying the intrinsic emission band consists of a doublet whose relative amplitudes depend on the analyzed areas. These variations may result from a matrix effect (differential absorption by the matrix) or from different mechanisms of photon generation as will be discussed later. A selected wavelength CL image at λ = 350 nm at the surface of the Tm-doped zircon shows an apparent increase in the Tm concentration in contradiction with the chemical analyses with the EPMA, while the CL image

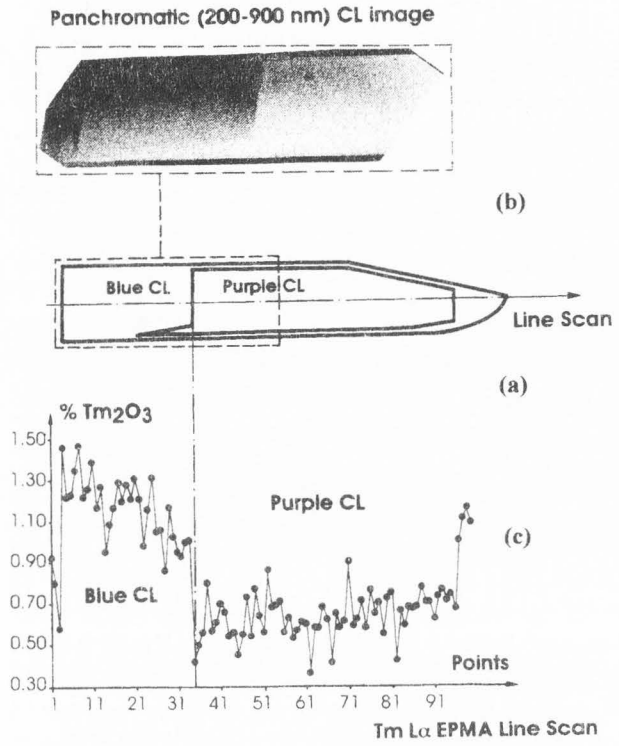

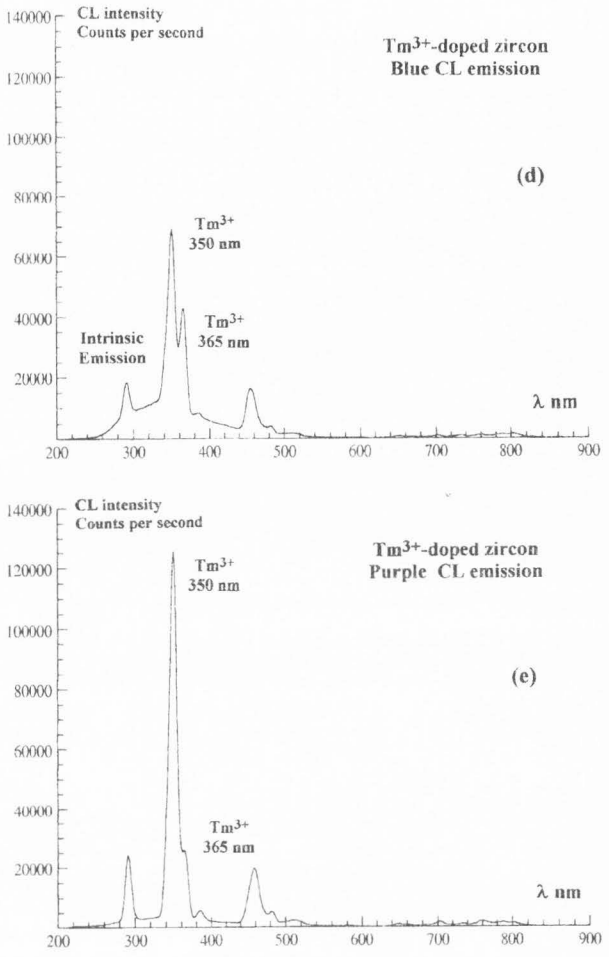

Figure 13. Polished Tm-doped zircon. (a) Schematic illustration of the areas exhibiting CL blue and purple CL hue in Figure 1. (b) Non-spectrally resolved CL image corresponding to the 200-900 nm interval. (c) EPMA Tm Lα quantitative line scans along the direction marked on the schematic view (a). CL emission spectra recorded at the end (d) and at the center (e) of the crystal.

---

at λ = 365 nm displays contrasts consistent with the spatial distribution of the Tm concentration.

The results for the Ce-doped and Tm-doped zircon crystals indicate that **the spatial distribution of the impurities is not a self-sufficient explanation to the change in contrasts of the CL images**. Furthermore, even for selected wavelength images associated with a characteristic emission of the REE activators, the contrasts of the CL images do not always show a positive correlation with the spatial distribution of a particular REE ion, i.e., the proportionality between the emitted characteristic CL intensity and the concentration of the activator may be not satisfied.

Relationship Between CL Contrasts and Charge Trapping Mechanisms

The change in brightness of the CL color cannot be simply correlated with the concentrations of the REE and P ions; the development of defect centers resulting from the presence of the P^{5+} ions (added to the flux in order to maintain the charge balance) must also be considered. The number of Si^{4+} + P^{5+} ions must be counter-balanced by the number of Zr^{4+} + $(REE)^{3+}$ ions. Due to an unsatisfactory charge compensation, electron and hole traps will be created leading to the development of electrical fields within crystals. As discussed by Cazaux (1986) and by Cazaux and Le Gressus (1991), the macroscopic surface and bulk electrostatic charging phenomena of insulators (such as silicate minerals) involve microscopic causes leading to charge trapping on energy levels located within the forbidden band-gap of the crystal. These electron traps, associated with crystal imperfections (vacancies, impurities, grain boundaries etc.) are involved in the production of the intrinsic CL emission. An indirect illustration of charge trapping mechanisms resulting from the simultaneous addition of the $(REE)^{3+}$ and P^{5+} ions can be obtained by comparing the Duane-Hunt limit on the X-ray spectrum with the incident energy. A Duane-Hunt limit lower than the incident energy indicates the existence of a retarding potential decreasing the kinetic energy of the incident electrons and modifying the electron distribution

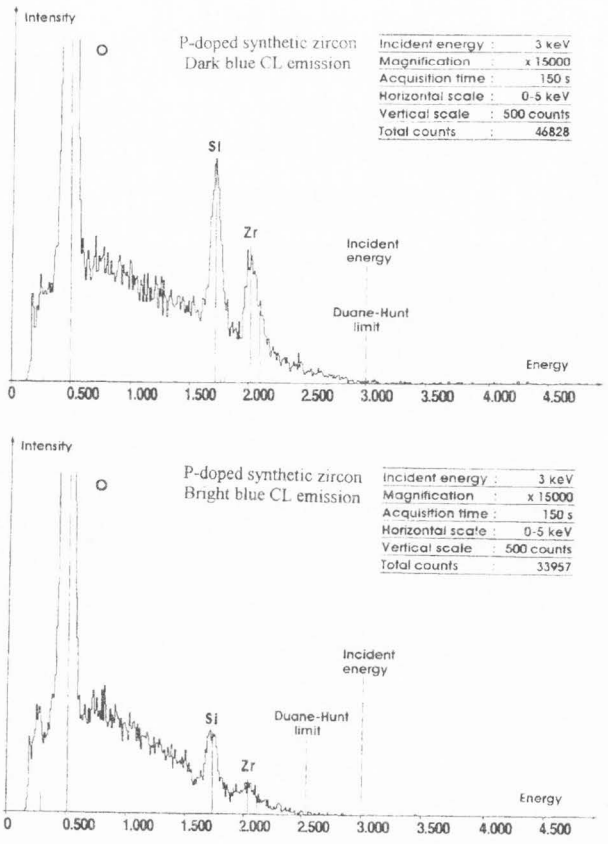

Figure 14. EDS spectra for a 3 keV incident energy recorded at the center (a) and at the end (b) of an uncoated P-doped zircon (crystal labelled Nd-doped in Fig. 1).

within the insulator compared with that for a conductive material. By means of an X-ray energy dispersive spectrometer (EDS), we tried to correlate the Duane-Hunt limits measured at the surface of the synthetic doped zircons with the changes of the intrinsic and extrinsic CL emissions. For this purpose, EDS spectra were acquired at the surface of the **uncoated** polished synthetic zircons. The maximum energy of the emitted X-ray photon was compared with the incident energy (3 keV). For EDS acquisition, the SEM was operated in the high vacuum mode. An electrostatic charge developed at the surface of the analyzed area (15,000X magnification) during the electron irradiation time for recording the first EDS spectrum. To remove this charge, the specimen surface was examined at low magnification (100X) at a pressure of 2 Torr in the specimen chamber; this step uniformly irradiates the area under examination. Following this examination, the SEM is again operated in the high vacuum mode for recording an EDS spectrum at another location (now at an uncharged surface). Also, for each analyzed specimen, an EDS spectrum was first recorded at a location having a low intensity structural defect induced CL emission prior to analyzing an area showing an intense intrinsic CL emission indicating a high density of defects (i.e., a high probability of charging under the electron irradiation).

X-ray spectra in Figures 14a and 14b correspond to the areas emitting, respectively, a dark and a bright blue CL emission at the surface of the P-doped zircon which was assumed to be doped with Nd but in which only P was incorporated as impurity. As previously illustrated in Figure 8, the P concentration is higher within the dark blue emitting area than at the surface of the crystal emitting the bright blue CL hue. At the surface of the area emitting a dark blue hue, the Duane-Hunt limit was equal to the 3 keV (same as the incident energy) indicating that no surface retarding potential developed (Fig. 14a). A retarding potential of about 500 V existed at the surface of the area emitting a bright blue hue as shown by the Duane-Hunt limit on the X-ray spectrum in Figure 14b. Furthermore, since these spectra have the same intensity scale, they show that the Si Kα and Zr Lα intensities are lower for the surface emitting the bright blue CL than the darker CL. These variations of the X-ray intensities are consistent with the existence of a retarding potential indicated by the changes of the Duane-Hunt limit values, i.e., the presence of the retarding potential leads to a decrease of the kinetic energy of the electrons scattered within the specimen. This effect is accompanied by a decrease in the ionization cross-section of the Si K and Zr L levels and a subsequent decrease of the X-ray photon yields with respect to those observed in absence of charging. The CL emission spectra of both areas emitting a bright and a dark blue CL hue (see Fig. 8c) consist of a broad UV band associated with lattice defects. The relative intensity of this band as a function of the analyzed area indicates a higher density of defects within the area exhibiting a bright CL hue than the dark blue CL emission. This relationship between the density of lattice defects and the intensity of the UV intrinsic emission band is consistent with the change in the Duane-Hunt limit observed at the two analyzed areas: (1) The retarding surface potential at the bright blue CL emitting area results from electron traps which are also responsible for the intense intrinsic CL emission. (2) No significant charging is detected at the dark blue CL emitting area indicating a low density of defects and subsequently, a low intensity of the host lattice CL emission.

The intensity of the CL emission within the UV blue part of the spectrum also correlates well with the Duane-Hunt limit as a function of the analyzed area of the Ce-doped zircon. The EDS spectra measured at the end (dark blue on the color image in Fig. 1, i.e., bright level on the polychromatic image in Fig. 11) and at the center

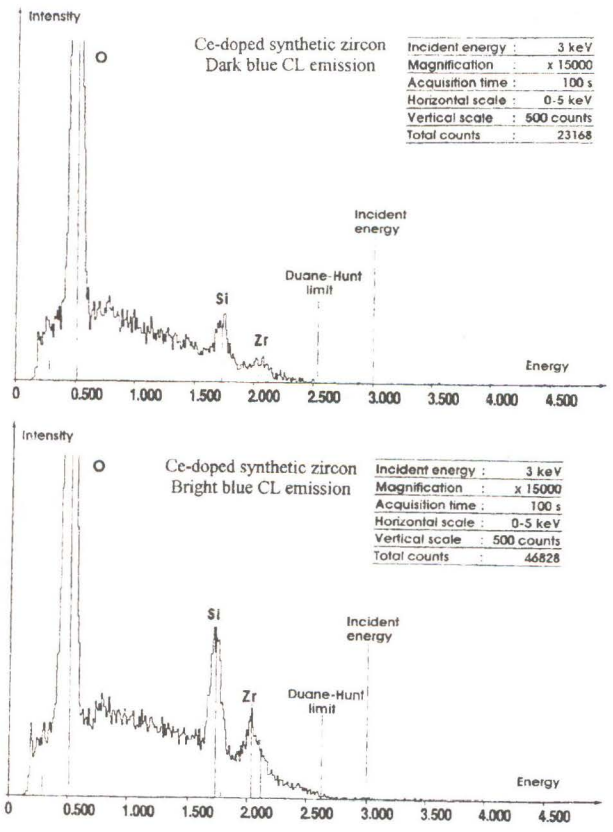

Figure 15. EDS spectra for a 3 keV incident energy measured at the center (a) and the end (b) of an uncoated Ce-doped zircon.

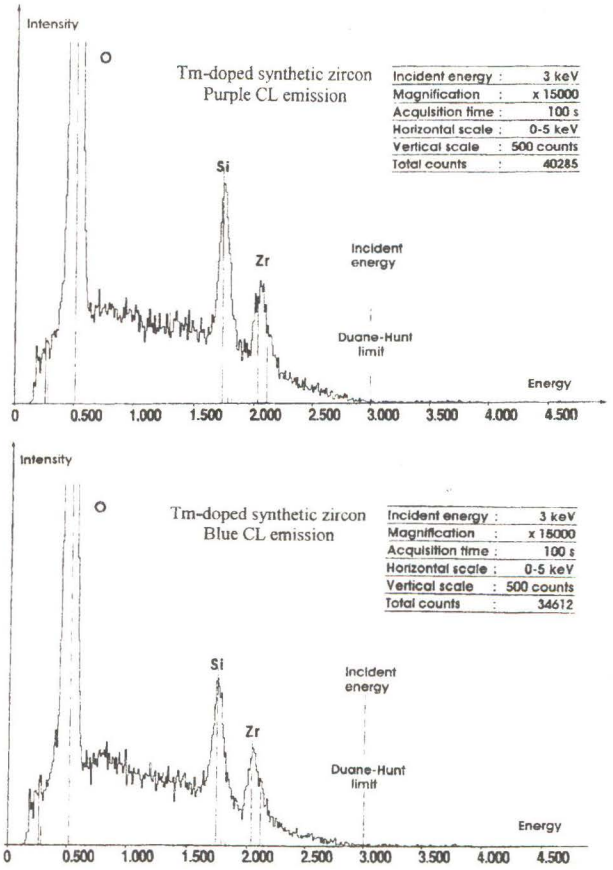

Figure 16. EDS spectra for a 3 keV incident energy measured at the center (a) and the end (b) of an uncoated Tm-doped zircon.

(bright blue on the color image in Fig. 1, i.e., dark level on the polychromatic image in Fig. 11) of the Ce-doped zircon are shown in Figures 15a and 15b, respectively. Both spectra show a difference in the Duane-Hunt limits compared to the incident energy. A higher retarding potential developed at the end of the crystal than at its center and consequently, the total number of counts measured during the 100 seconds acquisition time was lower for the measurement at the end of the crystal than for the measurement at the center of the crystal. These results indicate a higher density of electron traps at the end of the crystal than at its center; a result which is consistent with the CL emission spectra in Figure 12 indicating a lower integrated CL intensity over the 200-900 nm interval when measured at the center than when measured at the end of the Ce-doped zircon. Subsequently, the end of the polychromatic CL image exhibits a higher brightness than its center as observed in Figure 11. This consistency between the development of strong internal electrostatic fields and the variations in the integrated CL intensity (i.e., the brightness of the polychromatic CL image) is not valid for the color CL image (Fig. 1) where contrasts resulting from changes in the intensity of the emission are altered by the response function of the CL microscope (as discussed above).

Figures 16a and 16b show that for the Tm-doped zircon, no significant change in the Duane-Hunt limits were observed on the EDS spectra recorded at the areas emitting a blue (end of the crystal) or a purple (center of the crystal) CL (Fig. 1), respectively. However, internal electrostatic charges slowly increased during the irradiation time leading to a difference in the total counts accumulated during the irradiation time of both areas, as shown on the inserts in Figure 16. Fewer integrated counts are recorded at the end of the crystal than at its center indicating a higher density of defects in the former area compared with the latter. This variations in the density of defects shown by EDS analyses is consistent with the change in the intensity of the host lattice UV-blue CL emission (Fig. 13).

Discussion

To fully specify the observed color of the CL emis-

sion (direct viewing or recording on a photographic plate), it is necessary to consider: (1) the color associated with the dominant wavelength of the emission, (2) the saturation of the color which is the extent to which the color is pure and (3) the brightness or luminous intensity. As discussed by Remond *et al.* (1992), these three quantities leading to a quantitative interpretation of the observed CL emission can be calculated from chromaticity coordinates involving the sensitivity response factors of the receptor (eye or photographic plate) and the CL emission spectrum corrected for the instrumental response function. In the present study, the optical CL microscope was not equipped with a spectrometer and the observed colors were not quantified. The importance of the transmission of the CL microscope on the contrasts observed on the color photograph was illustrated by comparing the color images for the undoped (yellow CL color) and the P-doped zircon (blue CL color) shown in Figure 1. For these two crystals, the CL emission spectra (Fig. 9) consist of broad intense bands in the UV-blue region and only the intensities of these bands varied from a crystal to another one. Although the CL data of the undoped zircon did not show the presence of an intense band in the yellow part of the spectrum, the color CL image was dominated by a yellow hue. These observations led us to the conclusion that only photons with a wavelength greater than about 430 nm participate to the color of the CL image, owing to absorption through the successive materials along the optical path-length and to the sensitivity of the photographic plate used for the recording the color image. Furthermore, both the CL optical microscope and the CL spectrometer attached to the SEM have different response functions, making difficult the comparison between the CL color images and the non spectrally decomposed images. This effect is particularly marked for the case of the Ce-doped zircon whose CL hue is dominated by an intense intrinsic emission band occurring in the UV and blue part of the spectrum (Fig. 12). On the color image in Figure 1, the ends of the crystals appear darker that the center, while a higher brightness is observed on the non-spectrally (200-900 nm interval) decomposed CL image in Figure 11. CL emission spectra (Fig. 12) showed that for wavelengths lower than 430 nm or so, the CL integrated intensity measured at the ends of the crystal was higher than that measured at its center; the opposite situation was observed for wavelengths greater than the 430 nm threshold. The existence of the 430 nm wavelength threshold is responsible for the brightness changes as a function of the selected wavelength images of the Ce-doped zircon (Fig. 11).

In addition to instrumental factors, the contrasts of the CL images illustrate the spatial variations of the intensities measured at the specimen surface which, due to matrix effects, differ from those generated within the bulk materials.

The matrix effect includes the loss of CL intensity due to internal reflection on differently oriented crystallographic planes and to absorption phenomena along the CL photon path-length. The absorption effect depends on the optical constants of the material (refractive index n and extinction coefficient k) and on the incident energy which determines the depth distribution of the generated CL photons. For optical materials like insulators with REE or transition metal doping elements, the extinction coefficient is small relative to that for a semiconductor so that the absorption effect over the optical path-length is probably of a second order. Absorption effects resulting from a variation in the thickness of the crystals are not sufficient for explaining the bright CL intensity observed at the apex of most of the crystals (see color images in Fig. 1). An edge effect resulting from totally reflected CL beams on the differently oriented planes of the pyramidal faces at the apex of the crystals is probably responsible for the very bright CL intensity observed at the ends of the zircons. The matrix effect must also account for the anisotropy of the CL emission. As previously reported by Cesbron *et al.* (1995), the relative intensities of the intrinsic emission band and the REE characteristic CL peaks varied as a function of the crystal orientation with respect to the detector. We verified that the contrast on the polychromatic and selected wavelength images remained unchanged when the crystal was rotated around the incident electron beam direction, indicating that the contrasts of the CL images remained independent of the crystal orientation.

Spatially resolved X-ray analyses with the EPMA and the micro-PIXE showed that the contrasts observed on the CL images (color or polychromatic black and white images) correspond to variations in the distribution of the REE^{3+} and P^{5+} ions added to the synthetic zircons. However, the relationship between the brightness variations of the CL images and the concentration of the impurities is very complex. The CL intensity cannot be only explained on chemical composition but based on the consequences of electric charge disequilibrium resulting from composition changes.

To relate the intensity of a characteristic emission line with the concentration of a specific activator, it is necessary to simultaneously consider the transition probabilities of radiative and non-radiative charge recombination on the energy levels of the luminescent ions and the transition probabilities occurring on energy levels resulting from structural defects. During the electron irradiation, the luminescent centers associated with the lattice defects (UV emission) are preferentially excited and the intensity of the characteristic REE luminescence is deprived by the intensity of the intrinsic emission.

Such an effect could explain tentatively the non-proportionality between the intensity of a CL characteristic of the Tm^{3+} ions and the concentration of this doping element (Fig. 13).

In addition to the direct excitation of the luminescent centers by the incident energy, a mechanism similar to the energy transfer model described by Iacconi and Caruba (1980, 1984) and Iacconi (1995) studying the thermoluminescence properties of X-ray irradiated zircons must also be considered. According to the energy transfer model, the excitation of the REE^{3+} levels results from the absorption of the incident energy by the host lattice followed by energy transfer from the host lattice emission to the REE activator. Obviously, the energy transfer mechanism is only possible when the energy of the CL photon originating from defect centers is higher than the excitation threshold of the activator. The mechanisms of CL photon generation can be compared with the mechanisms of X-ray photons induced by electron bombardment, i.e., the direct excitation by the incident electrons and the secondary fluorescence induced by X-ray photons of sufficient energy being characteristic of elements in the specimen (energy transfer model for the case of the CL emission).

The transition probabilities of CL emission depend on the temperature of the specimen and on the nature of the excitation energy. As reviewed by Rémond *et al.* (1992), two sources: (1) thermal effect leading to two competitive mechanisms, i.e., thermal quenching and thermoluminescence and, (2) electrostatic charging phenomena resulting from charge trapping on pre-existing or induced defects must be considered for explaining the spatial variations of the CL signals as a function of the excitation conditions.

The relationship between the density of defects resulting from the addition of impurities different from the REE luminescent activator and the existence of retarding potentials reducing the kinetic energy of the incident electrons was shown by comparing the changes in the Duane-Hunt limits on the EDS spectra with the changes of the UV-blue CL emission. CL and EDS spectra for a P-doped synthetic zircon (Figs. 8 and 14) showed that the highest density of defect recombination centers (bright blue CL hue) corresponds to the presence of the highest retarding potential. The same correlation between the development of internal electric fields resulting from charge trapping mechanisms and the intensity of the UV-blue CL emission bands related to structural defects was also observed when both REE^{3+} and P^{5+} ions were simultaneously added, as illustrated for the case of the Ce-doped zircon (Figs. 12 and 15) and for the case of the Tm doped zircon (Figs. 13 and 16). These results indicate that the electric charge balance between the (REE^{3+} + Zr^{4+}) ions and the (Si^{4+} + P^{5+}) ions is not satisfied at the microscopic scale.

The development of internal electrical fields modifies the spatial and the energy distributions of the electrons in the insulators (CL production yield) and also induces beam damages (induced defects). As reviewed by Cazaux (1986, 1995), an electric field can develop in a coated insulator as a result of charge trapping mechanism on structural defects or as a result of an Auger mechanism. Beam damages in electron irradiated insulators involve two phenomena: (1) the charging effects leading to the distortion of the ionization depth distribution with respect to that for a conductive material and (2) the modification of the specimen composition resulting from the migration of mobile species driven by the electric field created inside the insulator. Remond *et al.* (1979) have reported on ionic diffusion induced by electron irradiation by combining CL and Auger electron spectroscopies. Electromigration resulting from the trapped charge induced electrical field following the electron irradiation has been illustrated by Jbara *et al.* (1996), who showed that negative species migrate towards the specimen surface and desorb into the vacuum. According to Jbara *et al.* (1996), the time exponential decay of the halogen X-ray signals, is directly related with the electric field change as a function of depth. Stevens Kalceff and Philips (1995a, b) identified some CL emission bands with irradiation-sensitive defects in natural and synthetic quartz specimens and showed that the formation of defects is accompanied by surface and sub-surface enrichment of the oxygen concentration with the development of outgrowths from quartz. Armstrong (1988) reported that quartz SiO_2 suffers radiation damage during electron bombardment with the EPMA, leading to a rapid increase in the O Kα intensity. Lineweaver (1963) and more recently Laval *et al.* (1985) reported that the beam-induced reduction effect leads to the formation of oxygen bubbles which evolve from glasses after their formation within the bulk materials exposed to the incident electrons. The ionization damages induced by the incident particles can modify the shape and the intensity of the CL host lattice emission bands. Similarly, the desorption of oxygen may also be responsible for the change in the O Kα emission band measured at the surface of some silicate and oxide materials after long irradiation time. Fialin and Remond (1993) and Fialin *et al.* (1994) showed that the shape of the O Kα emission peak also depended on transitions occurring on energy levels located in the forbidden bandgap of the crystal resulting from pre-existing or induced defects. Further investigations combining simultaneous analysis of the O Kα and CL emission bands as a function of the excitation conditions(incident energy, irradiation dose, temperature) should provide a better understanding of the radiative and non-radiative transitions

involving structural defects and the subsequent shallow levels localized in the bandgap of the energy diagram of the crystal.

For zircons, Cesbron *et al.* (1995) showed that the intensities of the CL peaks associated with structural defects varied as a function of the excitation conditions. These variations indicate that the density of defects was modified by the irradiation and that defects different than those resulting from the crystal growth conditions and from the addition of phosphorus and other possible impurities from the flux were also created as a result of ionization damages. However, it is still difficult to assign with certainty the emission bands in the UV-blue part of the spectrum to a specific impurity or defect. More particularly, the origin of the peak at 230 nm is still in debate and can be associated either with the edge emission band consistent with the 5.4 eV value of the zircon band gap as reported by Fielding (1970) or may be a host lattice emission band associated with lattice defects (Votyakov *et al.*, 1985, 1986). Assuming that the peak at 230 nm corresponds to the true intrinsic emission, the decrease of its intensity when the incident energy is decreased (Cesbron *et al.*, 1995) means that the probability of direct charge recombination through the band gap of the crystal is also decreased due to a preferential probability of charge recombination on energy levels resulting from crystal imperfections. Assigning the peak at 230 nm to the true intrinsic emission leads to the conclusion that the surface contains more defects than the core of crystal, while an opposite situation results from the assumption that the peak at 230 nm is associated with a structural defect recombination center, i.e., the intensity variations as a function of the incident energy mean that the surface contains a lower density of defects than the bulk crystal. For a constant incident energy, Cesbron *et al.* (1995) reported that the intensity of the peak at 230 nm relative to that of the peak at 290 nm increased by a factor of 2 when the electron beam current was increased from 10^{-9}A to 10^{-8}A. The variations of the CL intensity as a function of the irradiation dose are characteristic of a beam damage resulting in an increase of the density of defects.

The discussion above regarding the two possible origins of the peak at 230 nm (true intrinsic or defect induced emission) makes questionable the use of the now well-accepted "intrinsic emission" term for the UV-blue CL emission common to all silicate minerals. Direct charge recombination (intrinsic emission in the strict sense) and charge recombination on shallow levels in the bandgap have complementary probabilities to occur, leading to different intensity variations as a function of the excitation conditions. Both mechanisms must be clearly identified before obtaining a reliable interpretation of CL spectra. In the literature related to the theory of luminescence in crystals, the term intrinsic emission strictly refers to the mechanism of direct charge recombination, and using the same term independently of the width of the bandgap of the materials may lead to erroneous interpretation of CL spectra. For this reason, we recommend to designate the UV-blue emission of wide bandgap crystals as structural defect related CL emission or self-activated emission instead of intrinsic emission.

Conclusion

This study showed how complex the interpretation of the contrasts of CL images is, even for the case of monochromatic images at selected wavelengths characteristic of CL emission lines of REE^{3+} activators. Color CL images with a cold cathode electron gun attachment to an optical microscope provide an attractive illustration of heterogeneities at the surface of an apparently homogeneous crystals. However, in some instances, the contrasts of color CL images may differ from those observed on polychromatic or monochromatic CL images obtained with the SEM equipped with a CL spectrometer. These differences result from the optical transmission and the excitations conditions for each equipment used. It is necessary to account for matrix effects modifying the number of emitted CL photons with respect to the number of photons generated within the materials. Furthermore, the mechanisms of CL photon generation must be better understood before expressing the intensity of a characteristic CL emission line as a function of the concentration of the associated activator. For this purpose, time dependence studies of the CL and X-ray signals measured simultaneously as a function of the irradiation dose at the surface of metal coated and uncoated insulators maintained in a low or a high vacuum environment should allow us to investigate the role of pre-existing or induced defects on CL and soft X-ray emission spectra of wide bandgap crystals.

Acknowledgements

This research was partially supported by the DBT-INSU (CNRS) grant 4/06-4-15 to DO and FC. The authors thanks Drs. C. Yang (University of Lund, Sweden) and C. Choi (CNRS-CERI, Orleans, France) for the PIXE analyses.

References

Armstrong JT (1988). Accurate quantitative analysis of oxygen and nitrogen with a W/Si multilayer crystal. Microbeam Analysis. Newbury DE (ed.). San Francisco Press, San Francisco, USA. p. 301 (abstract).

Bresse JF, Rémond G, Akamatsu B (1996). Cath-

odoluminescence microscopy and spectroscopy of semiconductors and wide bandgap insulating materials. Mikrochim. Acta, in press.

Cazaux J (1986). Electrostatics of insulators charged by incident electron beams. J. Microsc. Spectrosc. Electron. **11**, 293-312.

Cazaux J (1995). The role of the Auger mechanism in the radiation damage of insulators. Microsc. Miceoanal. Microstruct. **6**, 345-362.

Cazaux J, Le Gressus C (1991). Phenomena relating to charge in insulators: Macroscopic effects and microscopic causes. Scanning Microsc. **5**, 17-27.

Cesbron F, Blanc P, Ohnenstetter D, Rémond G (1995). Cathodoluminescence of rare-earth doped zircons: Part I: Their possible use as reference materials. Scanning Microscopy Suppl. **9**,

Chapoulie R, Bechtel F, Borschneck D, Schvoerer M, Rémond G (1995) Cathodoluminescence of some synthetic calcite crystals, investigations on the role played by Cerium. Scanning Microscopy Suppl. **9**,

Fialin M, Rémond G (1993). Electron probe microanalysis of oxygen in strongly insulating oxides. Microbeam Analysis **2**, 179-189.

Fialin M, Rémond G, Bonnelle C (1994). New developments in electron probe microanalysis of oxygen in wide bandgap oxides. Microbeam Analysis **3**, 211-224.

Fielding PE (1970). Colour centers in zircon containing both Eu^{3+} and U^{4+} ions, Aust. J. Chem. **8**, 1513-1521.

Hanchar JM, Rudnick RL (1995). Revealing hidden structures: the application of cathodoluminescence and back-scattered electron imaging to dating zircon from lower crustal xenoliths. Lithos **36**, 289-303.

Iacconi P (1995). Thermoluminescence of zircon. Scanning Microscopy Suppl. **9**,

Iacconi P, Caruba R (1980). Trapping and emission centres in X-irradiated natural zircon. III. Influence of trivalent rare earth impurities. Phys. Stat. Sol. (a) **62**, 589-596.

Iacconi P, Caruba R (1984). Trapping and emission centres in X-irradiated natural zircon. Characterization by thermoluminescence. Phys. Chem. Mineral. **11**, 195-203.

Jbara O, Cazaux J, Rémond G, Gilles C (1996). Halogen ion electric field assisted diffusion in Fluorite and Polyvinyl chloride during electron irradiation. J. Appl. Phys., **79**(3), in press.

Laval JY, Delamarre C, Amamra MC, Broussaud D (1985). Influence of the intergranular microstructure of substituted nitrides on high temperature strength. J. Mater. Sci. **20**, 381-390.

Lineweaver JL (1963). Oxygen outgassing by electron bombardment of glass, J. Appl. Phys. **34**, 1786-1791.

Onasch CM, Vennedanne TW (1995). Disequilibrium partitioning of oxygen isotopes associated with sector zoning in quartz. Geology **23**, 1103-1106.

Rémond G, Le Gressus C, Okuzumi H (1979). Electron beam effects observed in cathodoluminescence and Auger electron spectroscopy in natural materials: Evidence for ionic diffusion, Scanning Electron Microsc., **1979**; I, 237-244.

Rémond G, Cesbron F, Chapoulie R, Ohnenstetter D, Roques-Carmes C, Schvoerer M (1992). Cathodoluminescence applied to the microcharacterization of mineral materials: A present status in experimentation and interpretation. Scanning Microsc. **6**, 23-68.

Rémond G, Gilles C, Isabelle D, Choi C, Azahra M, Rouer O, Cesbron F (1995). Electron and proton induced X-ray spectrometry: Two complementary spatially resolved analytical techniques in mineralogy. Appl. Radiat. Isot. 563-570.

Rouer O, Rémond G, Gilles C, Cesbron F, Choi C, Yang C, Malmqvist K (1995). Applications of electron and proton induced X-ray spectrometry to the localization of rare-earth elements in synthetic zircons. Mikrochem. Acta, in press.

Stevens Kalceff MA, Phillips MR (1995a). Electron irradiation induced outgrowths from quartz, J. Appl. Phys. **77**, 4125-4127.

Stevens Kalceff MA, Phillips MR (1995b). Cathodoluminescence microcharacterization of the defect structure of quartz. Phys. Rev. B **52**, 3122-3134.

Votyakov SL, Krokhalev VY, Krasnobaev AA (1985). Zircon recombination luminescence. J. Appl. Spectrosc. **42**, 633-638.

Votyakov SL, Ivanov IP, Krasnobaev AA, Krokhalev VY, Korzhinskaya VS (1986). Luminescence-spectral properties of zirconium orthosilicate prepared by hydrothermal method. Inorg. Mater. **22**, 239-244.

Discussion with Reviewers

M. Phillips: Data in Figure 2 show single peaks at 485 nm and 580 nm for the Dy^{3+} doped zircon, we see 8 peaks at 485 nm with approximately 0.2 nm bandpass. What CL spectral resolution did you use?

Authors: We showed (Rémond *et al.*, 1992) that the 485 nm and 580 nm peaks for Dy3+ ions consist of several fine features. By the use of a multichannel spectrometer equipped with a grating monochromator and an intensified photodiode array as a detector, each single peak was decomposed into multiple features when the number of grooves per millimetre (gr/mm) of the grating was increased from 150 gr/mm to 300 gr/mm. With the 300 gr/mm grating and a 512 photodiode array, the

wavelength resolution was 0.3 nm, allowing us to resolve the 485 nm peak into three peaks, while as reported by the reviewer, height peaks were measured with a 0.2 nm wavelength resolution. In the present study, a scanning spectrometer equipped with a 1200 gr/mm grating was used. The resolution increases when the width of the spectrometer slits is decreased. A wavelength resolution of 4 nm (0.5 mm slit width) was used for obtaining reference spectra of the synthetic zircon doped with a single REE (Cesbron *et al.*, 1995). This resolution was sufficient for a qualitative interpretation of CL spectra but must be increased for identifying all fine structures. However, reducing the slit width is accompanied by an important loss of the measured CL intensity so that the incident electron beam current must be increased. Increasing the beam current has for consequence to increase the risk of creating beam damages. For CL imaging, the slit width was adjusted in order to improve the CL signal intensity and a 8 nm wavelength resolution (1 mm slit width) was used. The CL spectra were obtained for the same instrumental conditions and consequently, fine structures on the CL peaks in Figure 2 were not resolved.

M. Phillips: How reproducible is the Duane-Hunt cut-off position?

Authors: Charging phenomena depend on many instrumental and experimental factors so that, even if the electron beam current is accurately reproducible, it is almost impossible to obtain reproducible absolute Duane-Hunt limit values from successive measurements. According to the analytical procedure described in text, two successive measurements, A1 and A2, carried out at the same location, A, of the specimen surface kept in high vacuum, led to measured potentials in the same order of magnitude, $\Delta VA1 \approx \Delta VA2$, when the specimen surface was irradiated in a low vacuum environment between the two successive EDS acquisition. The irradiation in a low vacuum environment has partly canceled the excess of surface charges resulting from the first irradiation in a high vacuum environment. Because a 3 keV incident energy was used for EDS analyses, the thickness of the charged layer below the specimen surface was thin enough for permitting the restoration of the neutrality of the pre-irradiated surface due by the surrounding gas molecules during the low vacuum irradiation. With the experimental procedure used, absolute Duane-Hunt positions were not measured, but the important result is that the difference in the Duane-Hunt positions measured at several locations at the surface of the same specimen was reproducible.

M. Phillips: Have you compared focussed probe and defocussed probe CL data?

Authors: The local changes of the internal electric fields modify both the kinetic energy and the spatial distribution of the electrons scattered in the insulating zircon crystals and subsequently modify the yield of the CL photon generation. More particularly, the charge trapping mechanisms depend on the density of incident particles and different CL properties will be observed when the diameter of the incident electron beam will be varied. It has been shown that natural zinc sulfide minerals exhibited a red CL emission when the incident beam of the EPMA was unfocused and that the CL emission turned to a blue-green hue when the specimens were irradiated with a stationary focused beam (G. Rémond: Applications of cathodoluminescence in mineralogy. J. of Luminescence, 1977, 15 (2), 121-155). The dependence of CL properties of zircon crystals must be studied in relation with the study of charging phenomena and beam damages as a function of the excitation conditions.

M. Phillips: Are structural defects created by a focussed probe? Do you see new CL peaks following electron irradiation?

Authors: Studying an undoped zircon, Cesbron *et al.* (1995) showed that the intensity of the peak at 230 nm was strongly dependent on the incident energy and beam current. The peak at 230 nm was no longer detectable when a 3 keV incident energy was used, indicating a change in the density of defects as a function of depth below the specimen surface. However, for a constant incident energy, Cesbron *et al.* (1995) also showed that the intensity of the peak at 230 nm relative to that of the other peaks in the UV-blue region also varied as a function of the electron beam current, indicating the existence of beam damages. In the present study, we also observed beam damages when CL spectra were measured at beam spots of a stationary focussed beam and by varying the dimensions of the irradiated areas by a focussed scanning beam. The wavelength resolution was not sufficient to reveal possible additional features on CL spectra as a function of the incident electron dose. However, depending on the analyzed areas, the relative intensities of the CL emissions associated with structural defects were changed as a function of the irradiation dose. Charging phenomena (as well as thermal increase) may lead to a variation of the yield of the CL photon generation as a function of the excitation conditions. Charge trapping is a dynamically phenomenon due to two competitive mechanisms, i.e., trapping and detrapping of electrons. Time resolved analysis of all signals resulting from the electron beam irradiation is necessary for determining the analytical strategy to be used for the microcharacterization of insulators by means of electron beam based techniques.